ELSEVIER

Journal of Chromatography A, 691 (1995) 273–283

JOURNAL OF CHROMATOGRAPHY A

High-performance liquid chromatography of amino acids, peptides and proteins CXXXIX[☆]. Impact of operating parameters in large-scale chromatography of proteins

Qi-Ming Mao, Ian G. Prince, Milton T.W. Hearn*

Centre for Bioprocess Technology, Monash University, Clayton, Victoria 3168, Australia

Abstract

Large-scale chromatography has been playing an important role in downstream treatment processing in biotechnology. In order to improve the productivity, the throughput of the chromatographic equipment was often increased by increasing the flow-rate and/or by increasing the column sample loading. This paper reports the results of a study on the impact of these and other operating parameters in affinity and ion-exchange chromatographic columns when used for protein purification. A sectional model was developed to predict protein adsorption processes in a packed column. The formulations of this mathematical model are presented in the Appendix. The present study was carried out with computer simulation based on this model and using data obtained from laboratory-scale columns. This model can simulate both the adsorption and washing stages of the protein purification process for both porous and non-porous particles. The effects of changing operating parameters were simulated and contour plots were generated for the easy identification of these effects. It was shown that both flow-rate and column loading can have a considerable impact on the processing rate and the yield of the column. As for the column capacity utilization, the impact of changing flow-rate is not significant at column loading of less than 80% in the test case. It was suggest that the present investigation provides a systematic predictive strategy which will greatly reduce the need for expensive, labour-intensive and time-consuming experimental work during process scale-up.

1. Introduction

The importance of using chromatographic methods for the large-scale purification of high value proteins has been extensively realized over the past decade [1–3]. Competitive commercial pressures involved in product development now mean that improved approaches to process scale-up and optimization are required [4–9]. As a consequence, the synergy between process simulation with mathematical models and directed experimental design to achieve essential data for the estimation of optimum parameters has become increasingly evident, particularly when iterative approaches based on physically relevant models are employed. The present investigations address a practical procedure developed in this Centre for the selection of operating parameters in ion-exchange or affinity chromatographic beds

* Corresponding author.

[☆] For Part CXXXVIII, see Ref. [21].

0021-9673/95/$09.50
SSDI 0021-9673(94)00876-0

as part of a large-scale protein purification process. Computer simulations, generated from the analysis of the concentration–time profiles and derived from batch and packed-bed adsorption and washing stage experiments with different adsorbents and mixtures of proteins, form part of the selection procedure for the appropriate choice of fluid velocity, sample loading volume and concentration and column length and diameter. The primary objective of these investigations was to maintain maximum production rates for these stages with packed-bed systems during scale-up, whilst ensuring that the basic requirements of product yield and purity at predetermined levels were achieved. Increasing the mobile phase flow-rate and increasing the column loading are the main avenues to achieve high production rates. As such, the study of the effect of these two parameters formed a major part of the current investigation.

As part of this interactive scale-up procedure involving experimental measurements of protein adsorption behaviour and simulation of this behaviour under a defined set of conditions, a mathematical model developed in this Centre was used to fit the experimental breakthrough curves to extract the surface interaction rate constants. This model is capable of independently addressing both the external mass transfer and surface interaction, yet retains the simplicity of analytical solution. The adsorption and washing behaviour of the column under various operating conditions were simulated and compared with the experimental behaviour. The product yield, column capacity utilization and production rate were then calculated.

These data can then be meshed with the specific process economics to yield an overall optimum outcome. The region of optimum large-scale operation can then be established on the basis of limited small-scale experimentation.

2. Experimental

Experimental data from a number of protein–sorbent systems studied in this Centre were used in the current study. Specific details on the materials, methods, equipment set-up and operating procedures have been published elsewhere [10–13]. Preliminary results on the simulation of the adsorption of lysozyme to Cibacron Blue F3GA biomimetic affinity systems have been presented previously for both non-porous [8,14] and porous [9] particles. Experimental results for two additional systems are reported in this paper. In one of the systems studied the matrix used was an iminodiacetic acid–copper(II) [IDA–Cu(II)]-modified 1.5-μm diameter non-porous silica adsorbent. The adsorbates used were concanavalin A and hen egg-white lysozyme. The column used was 19 mm × 4 mm I.D. The detailed procedure for the preparation of the IDA adsorbent and other experimental details can be found elsewhere [11,12]. The data for the human serum albumin (HSA)–DEAE-Trisacryl M ion-exchange system were measured [13] in a 5-mm I.D. column (Pharmacia 5/5 HR). HSA was supplied as a 21% solution from Commonwealth Serum Laboratories (CSL) (Melbourne, Australia). DEAE-Trisacryl M ion-exchange resin (particle size 40–80 μm) was purchased from Australia Chemical Co. (Melbourne, Australia). The computer programs (BEDSTP and BEDSTS) using the sectional model described in the Theoretical considerations section and the Appendix were written in FORTRAN. The computation was carried out using an IBM PC compatible machine linked to a VAX 8700 mainframe computer. The figures were drawn with a Macintosh computer.

3. Results and discussion

3.1. Theoretical considerations

Owing to the complexity of the protein–sorbent systems which occurs in large-scale chromatography, it is not possible to identify ideal optimum operating conditions from a single analytical chromatographic experiment. This investigation thus aimed at defining an optimum region of a set of parameters within which the predetermined production criteria can be

achieved. A large number of simulations will be required, hence a simple yet rigorous mathematical model is essential. For example, the model should still be able to take into account the effects of all major rate-limiting factors and also accommodate the influence of different adsorption isotherms.

A sectional model of a chromatographic column developed in this Centre was used in the optimization study reported in this paper. In this model, the column is divided into a series of sections. Each section is then treated as a well mixed tank, with the equations used in the batch adsorption model developed earlier [15] forming the key algorithm of the model. This model is similar to the discrete cell model or the discrete stage model available in the literature [16,17]. In this type of model, the flow conceptually is treated as non-continuous parameter. According to this model, in each section of the column the fluid containing the solute protein (adsorbate) of interest is brought into contact with the adsorbent and interaction is allowed to occur for a period of time, Δt. At the end of each time increment, the content of the liquid (mobile) phase in each section is transferred to the next section. The time increment Δt is calculated as $\Delta t = L/U^*n$ where L is the column length, U the superficial velocity (linear flow-rate) of the fluid and n the number of the sections.

For adsorption with fresh or regenerated adsorbent particles, the initial adsorbate concentration in the solid (stationary) phase is zero for all the sections at the beginning of the process, and the column is assumed to be saturated with buffer solution. For the adsorption stage, the initial adsorbate concentration in the liquid phase is equal to C_0, the inlet concentration. For washing and elution stages, $C_0 = 0$.

The basic assumptions for rate limiting steps in the adsorption process are the same as those used in our non-porous particle adsorption model for a finite bath [15]. This treatment also permits other types of isothermal behaviour, e.g., Freundlich or multi-component Langmuirean isotherms to be accommodated. However, for the purpose of the present discussion only a single-component non-linear Langmuirean isotherm will be discussed. In this simple case, the assumptions are: (a) the transport of adsorbate from the bulk fluid to the surface of the particle can be described by a film resistance mechanism and (b) the interaction between the adsorbate and the adsorption site at the particle surface can be described by a Langmuir-type process. In addition, as each section is assumed to be well mixed, the concentration of the adsorbate in the liquid phase is assumed to be uniform throughout that section.

For the case with porous particles, a linear driving force approximation was used to describe the mass transfer of the adsorbate in the liquid phase from the entrance of the pores at the external surface to the particle internal surface. With this approximation, the pore fluid can be treated as a mass transfer medium rather than a separate phase, thus enabling it to be combined with the bulk fluid in the overall mass balance. At the end of each time increment, the pore fluid was assumed to remain stagnant, and only the bulk fluid was transferred to the next section.

With the above assumptions and initial conditions, the concentrations of the adsorbate in both the liquid and solid phases can be calculated. The liquid-phase concentration in the last section, C_n, is the outlet concentration. The concentration–time plot, i.e., the breakthrough curve, can then be constructed. As the concentrations in each section were stored for each complete time cycle during the calculation, the axial concentration profiles can also be produced for any particular time. Detailed formulation and derivation of the model and its solution are presented in the Appendix.

One of the key variables in the sectional model is the number of the sections, n. It was found that when n was larger than 16 in the test case, the effect of "numerical dispersion" was negligible and the breakthrough curves produced by the sectional model and the analytical solution of a packed bed [14] were synonymous and overlapped. The advantage of this model is thus its versatility. The adsorption stage may be terminated at any time without causing any difficulty in the calculation of the time–concentration curves in the washing stage. Another

important feature is that non-linear Langmuir adsorption isotherms were assumed.

3.2. Comparison of experimental and simulated data

The comparison of calculated and the experimental breakthrough curves is a favoured method by many researchers and has often been used in the validation of mathematical models of protein adsorption–desorption behaviour with chromatographic adsorbents and in extracting system parameters for further simulation [14,18–20]. The same approach was used in this study. Fig. 1 shows the result for the concanavalin A–IDA–Cu(II) adsorption system. Three concentrations of concanavalin A were used, i.e., $C_0 = 0.092$, 0.053 and 0.011 mg/ml. Other parameters were $q_m = 2.9$ mg/ml solid, $K_d = 0.0366$ mg/ml and $U = 0.66$ mm/s [12]. A reasonable fit was obtained between the predicted and experimental breakthrough curves for all three protein concentrations. The breakthrough curves calculated for this non-porous particle system by the sectional model were indistinguishable with the curves generated with the non-porous particle adsorption model (NPPAM) published previously [14]. As the model simulation for a non-porous particle system using the NPPAM model under different operating conditions has been presented previously, this paper will concentrate on the model simulation using the sectional model for a porous particle system.

Fig. 2 shows a typical curve fit of our model prediction to the experimental breakthrough curve for the albumin (HSA) adsorption to DEAE-Trisacryl M, which is a porous ion-exchange resin. The parameters used were column length = 13 mm, $C_0 = 1.5$ mg/ml, $q_m = 44$ mg/ml bed, $K_d = 0.0179$ mg/ml and $U = 0.42$ mm/s [13]. Although the model predictions fit experimental data reasonably well in these two figures, the agreement between the predicted and experimental breakthrough curves for some other situations studied was not as complete. For example, as discussed previously [14,15], complicated mass transfer and surface interaction processes, e.g., aggregation, multilayer formation and surface reorientation at high protein concentrations in the microenvironment of the adsorbent, may be the cause of divergences between the predicted and experimental breakthrough curves, since these phenomena have not been incorporated in the present model.

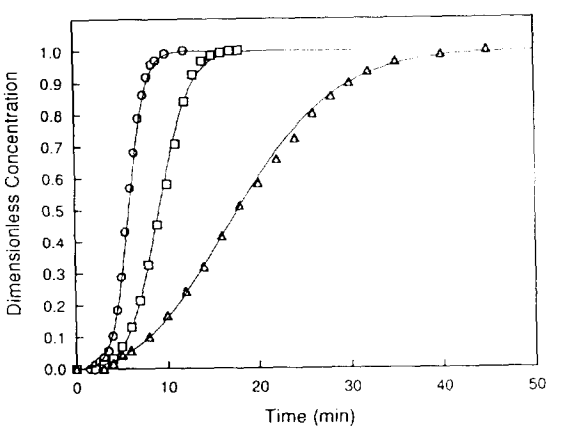

Fig. 1. Predicted (lines) and experimental (points) breakthrough curves for the adsorption of concanavalin A on an IDA–Cu(II)-modified 1.5-μm diameter non-porous silica adsorbent for three concentrations of concanavalin A, i.e., C_0 = (○) 0.092, (□) 0.053 and (△) 0.011 mg/ml. The column used was 19 mm × 4 mm I.D. Other parameters: $q_m = 2.9$ mg/ml solid; $K_d = 0.0366$ mg/ml; $U = 0.066$ cm/s.

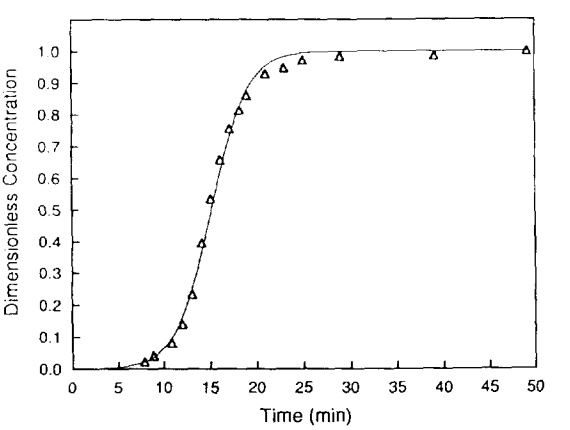

Fig. 2. Predicted (line) and experimental (points) breakthrough curves for the adsorption of human serum albumin (HSA) on DEAE-Trisacryl M ion-exchange sorbent. Column, 13 mm × 5 mm I.D.; $C_0 = 1.5$ mg/ml; $q_m = 44$ mg/ml bed; $K_d = 0.0179$ mg/ml; $U = 0.042$ cm/s.

3.3. Simulations of the effects of operating parameters

For most simulations, a column length of 100 mm was used. For the results shown in Figs. 4–11, a constant washing volume of ten column void volumes at a constant liquid velocity of 0.5 mm/s was employed. The washing stage was included to provide a more realistic simulation and a detailed discussion on this consideration has been presented previously [9]. The number of sections, n, was set as 20. Other parameters used are the same as for Fig. 2.

Although the study of breakthrough curves (frontal analysis) will provide detailed information about the behaviour of the chromatographic system in question, the availability of experimental breakthrough curves is often restricted to the laboratory-scale columns. Experimental results with process-scale chromatographic beds are often not reported in the literature because of issues of commercial sensitivity or simply because most industrial practitioners still underutilize the total capacity, preferring zonal elution. In a practical protein purification column, only a finite sample volume will be applied to the column and the breakthrough may not occur before the loading (adsorption) stage terminates. Therefore, the adsorption behaviour of large-scale columns has historically been studied largely from model simulation based on data acquired with small-scale, laboratory columns. The current study has concentrated on the sample loading volume and flow-rate as the main operating parameters owing to their practical importance.

It was well known that an increase in the flow-rate causes the spreading of the breakthrough curves due to the dispersion of adsorbates within the solid (stationary) phase [14,18]. With the assistance of the sectional model, this phenomenon can be simulated. Fig. 3 shows the effect of flow-rate on the axial concentration profiles in the solid phase of the bed when the same sample volume was loaded. At a very low flow-rate (5 ml/min), the concentration front in the solid phase is sharp. More than half of the column has been saturated but there is no adsorbate in the last 20% of the column. When

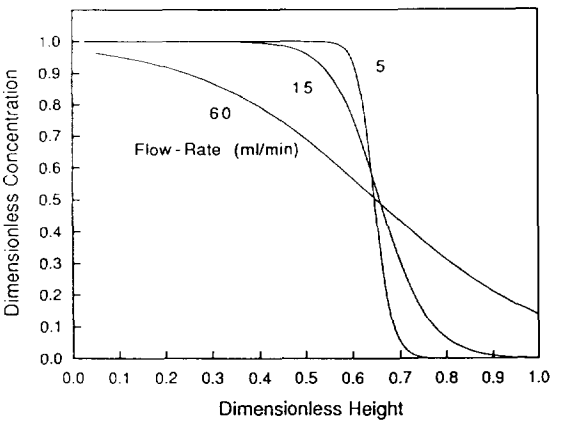

Fig. 3. Concentration profiles in the solid phase at different flow-rates for the same column sample loading for the HSA–DEAE-Trisacryl M ion-exchange system.

the flow-rate was increased to 15 ml/min, the saturated section reduced and the adsorbate migrated throughout almost the whole length of the column. For these two cases, no breakthrough was detected. For 60 ml/min, the breakthrough occurs before any part of the column becomes saturated.

The effects of flow-rate and column height on the maximum loading volume are shown in Fig. 4. The column was loaded to the point just

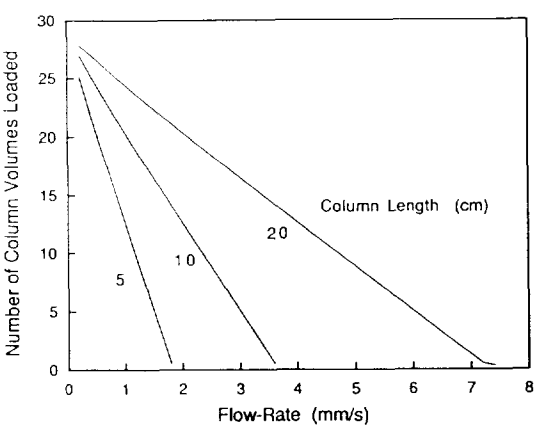

Fig. 4. Maximum column sample loading versus superficial liquid velocity for different column lengths at a fixed effluent concentration (0.1% of inlet concentration) for the HSA–DEAE-Trisacryl M ion-exchange system.

before breakthrough occurs ($C/C_0 = 0.001$). Under this condition (constant effluent concentration), the maximum loading volume, as shown, increases with increasing column length and is a linear function of the flow-rate. The effects on processing rate are shown in Fig. 5. The processing rate can be defined as the amount of protein retained after washing per unit volume of resin per unit processing time. Similarly to the results of earlier investigations reported from this Centre [8,9] and elsewhere [3,18], there exists an optimum flow-rate at which a maximum processing rate can be achieved. This optimum flow-rate is higher for the longer column but the value of maximum processing rate is higher for the shorter column [9,18].

The effects of column loading on processing rate are shown in Fig. 6. The column loading value used was defined as the percentage of the attainable column adsorption capacity. For the range where column loading is less than 100%, the processing rate increases with the increase of column loading and flow-rate. The yield, which is defined as the percentage of total protein applied to the column retained after washing, decreases with the increase of both flow rate and column loading, as shown in Fig. 7.

The operating range and the limitations of the two main operating parameters can be shown more clearly in the derived contour plots. From Fig. 8, it can be seen that high processing rates occur only at the top-right hand corner where both the flow-rate and the column loading are high. The high yield, however, is restricted to the low flow-rate and relatively low loading region, as shown in Fig. 9. Owing to the asymptotic nature in the calculation of the yield values by the sectional model, a value of 99.999% yield was chosen to be an approximation of 100%

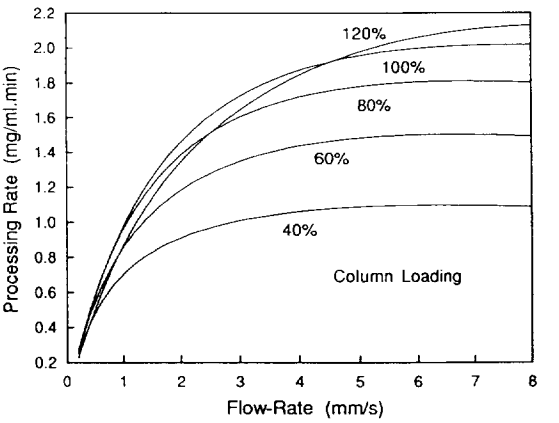

Fig. 6. Processing rate versus superficial liquid velocity at different column loadings (as percentages of the attainable column adsorption capacity) for the HSA–DEAE-Trisacryl M ion-exchange system.

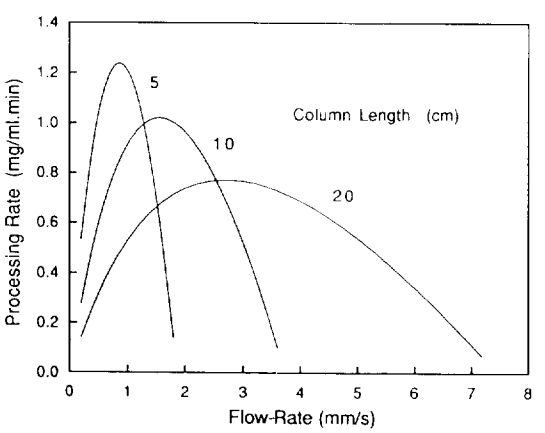

Fig. 5. Processing rate versus superficial liquid velocity for different column lengths at a fixed effluent concentration (0.1% of inlet concentration) for the HSA–DEAE-Trisacryl M ion-exchange system.

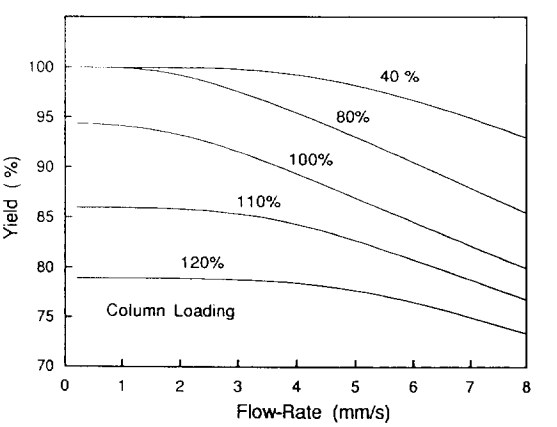

Fig. 7. Product yield versus superficial liquid velocity at different column loadings (as percentages of the attainable column adsorption capacity) for the HSA–DEAE-Trisacryl M ion-exchange system.

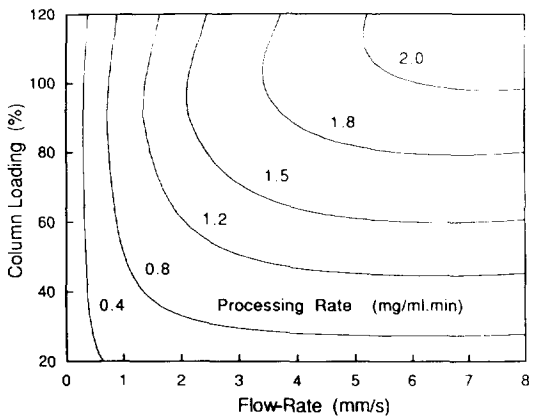

Fig. 8. Effects of liquid velocity and column sample loading on the processing rate (mg/ml · min) of an HSA–DEAE-Trisacryl M ion-exchange chromatographic column.

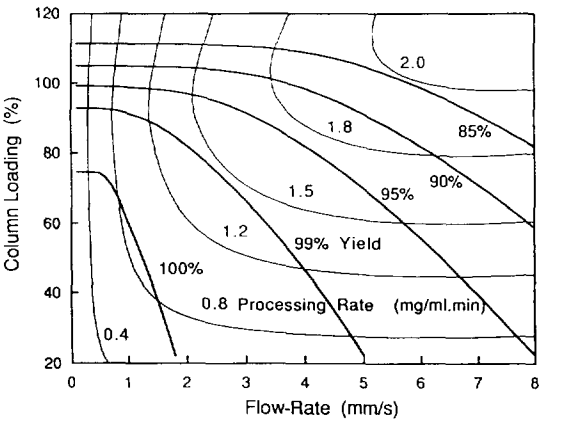

Fig. 10. Operating regions based on the product yield and processing rate for an HSA–DEAE-Trisacryl M ion-exchange chromatographic column.

yield. It can be seen that in order to improve the yield from 99% to 100%, the flow-rate has to be reduced to less than half and the column loading may also have to be reduced. This interdependence becomes more evident when these two sets of curves are plotted together, as shown in Fig. 10. When the yield was allowed to drop from 100% to 99%, this 1% decrease resulted in a 60–70% increase in the processing rate. Depending on the actual yield requirement of the production, the expected processing rates and the operating range of the flow-rate and column loading can thus be easily estimated from these plots.

Another production criterion worth mentioning is the column capacity utilization, which can be defined as the percentage of the attainable column capacity used in the adsorption–washing cycle [9]. This criterion is important as it directly affects the column life and the equipment cost. High column capacity utilization is generally preferred. As shown in Fig. 11, changes in the flow-rate have little effect on the capacity utilization when the column loading is low. When the

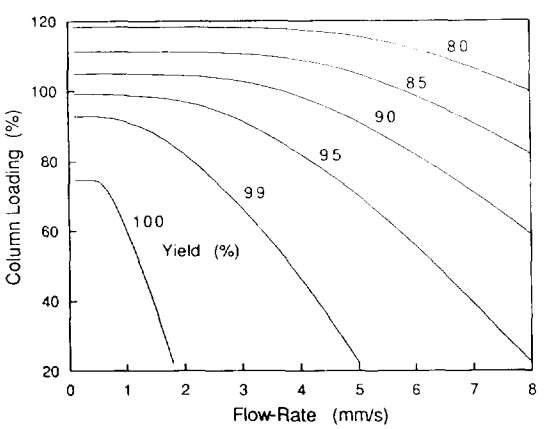

Fig. 9. Effects of liquid velocity and column sample loading on the product yield of an HSA–DEAE-Trisacryl M ion-exchange chromatographic column.

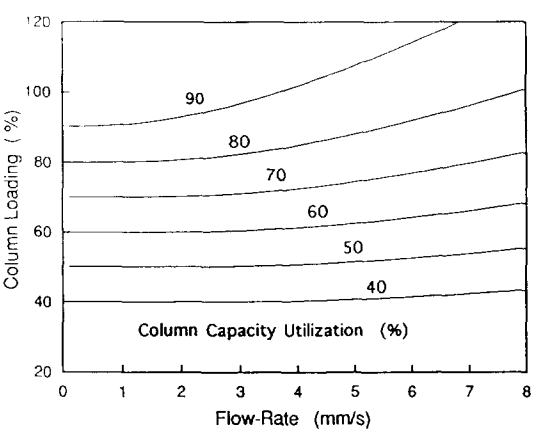

Fig. 11. Effects of liquid velocity and column sample loading on the column capacity utilization level of an HSA–DEAE-Trisacryl M ion-exchange chromatographic column.

column loading is higher than 80% in this particular example, however, the increase in flow-rate will result in a decrease in the column capacity utilization.

4. Conclusions

The results of this study clearly demonstrate that the operating parameters involved in the chromatography of proteins, such as flow-rate and column sample loading, can have a significant impact on the outcome of the process. Whilst higher flow-rates will result in a higher processing rate, the yield drops with increase in flow-rate. In large-scale processes, the production rate will be a primary determinant, but the requirement for high yield and column capacity utilization must also not be overlooked. The final balance of these factors will depend on the process economics. Selection of optimum operating parameters thus represents a critical compromise between several variables. The procedures currently under development in this Centre can offer assistance in these aspects. The present investigation provides a systematic predictive strategy which greatly reduces the need for expensive, labour-intensive and time-consuming experimental work during process scale-up.

Symbols

a	external surface area per unit volume of adsorbent particles
A	parameter defined by Eq. A10
B	parameter defined by Eq. A12
C_i	adsorbate concentration in the liquid phase in section i
$C_{i,0}$	initial adsorbate concentration in the liquid phase in section i
$C_{p,i}$	adsorbate concentration in the pore fluid in section i
$C_{T,i}$	equivalent adsorbate concentration when total amount of the adsorbate in the system was assumed in the liquid phase in section i
C_i^*	intermediate adsorbate concentration in the liquid phase at (1) external surface of the particles in section i for the case with non-porous particles and (2) internal surface of the particles in section i for the case with porous particles
C_n	adsorbate concentration in the liquid phase in the last section, which represents the outlet adsorbate concentration
C_0	inlet concentration of adsorbate in the liquid phase
k_1	forward surface interaction rate constant
K_d	adsorption equilibrium constant
K_e	overall effective liquid-phase mass transfer coefficient
K_f	liquid-side film mass transfer coefficient
L	column length
M	parameter defined by Eq. A9
n	number of the sections in the sectional model (Eq. A1)
q_i	adsorbate concentration on the solid phase in section i
q_m	maximum solid adsorption capacity
$q_{i,0}$	initial adsorbate concentration on the solid phase in section i
R_0	particle radius
R_v	volume ratio of solid phase to liquid phase
Δt	time increment which is the residence time of bulk fluid in any one section
U	superficial velocity (linear flow-rate) of the fluid
x_1	positive root of quadratic Eq. A11
x_2	the other root of Eq. A11
ε	volume fraction of liquid phase in the column
ε_p	particle void fraction

Acknowledgements

These investigations were supported by the Australian Research Council and a research grant provided by CSL as part of the Industry Research and Development (IRD) board funding programme of the Department of Industry, Trade and Regional Development. The assistance of Dr. H.-J. Wirth in the acquisition of the

adsorption data with the non-porous adsorbents is greatly appreciated.

Appendix: the sectional model

In this model the chromatographic column is assumed to be divided into a series of sections. Each section is then treated as a well mixed tank. In each section the fluid containing the solute protein (adsorbate) of interest is brought into contact with the adsorbent and interaction is allowed to occur for a period of time Δt. At the end of each time increment, the content of the liquid phase in each section is transferred to the next section. The time increment Δt is calculated as

$$\Delta t = \frac{L}{Un} \tag{A1}$$

where L is the column length, U the superficial velocity of the fluid and n the number of the sections. The interaction between the adsorbate and the adsorption site at the particle surface is assumed in the treatment described below to be governed by a Langmuir-type isothermal model, but other isothermal models can be also employed. As each section is assumed to be well mixed, the concentration of the adsorbate in the liquid phase is uniform throughout the section.

Adsorption with non-porous particles

The overall mass balance for the adsorption with non-porous particles in a section i is

$$\varepsilon C_i + (1-\varepsilon)q_i = \varepsilon C_{T,i} \tag{A2}$$

where C_i is the adsorbate concentration in the bulk of the liquid phase, q_i is the adsorbate concentration on the solid phase, ε is the volume fraction of liquid phase in the column, which is assumed a constant throughout the column and the variable $C_{T,i}$ is the equivalent total adsorbate concentration when the total amount of the adsorbate in that section is assumed only in the liquid phase. $C_{T,i}$ can be calculated from

$$C_{T,i} = C_{i,0} + R_v q_{i,0} \tag{A3}$$

where $C_{i,0}$ is the adsorbate concentration in the liquid phase at the beginning of the time increment, $q_{i,0}$ is the adsorbate concentration in the solid phase at the beginning of the time increment and R_v is the volume ratio of the solid phase to the liquid phase, i.e. the phase ratio (often represented as Φ):

$$R_v = \frac{1-\varepsilon}{\varepsilon} \tag{A4}$$

The differential form of Eq. A2 then can be expressed as

$$\frac{dC_i}{dt} + R_v \cdot \frac{dq_i}{dt} = 0 \tag{A5}$$

As in the case with the non-porous particle adsorption model [14,15], the transport of adsorbate from the bulk fluid to the surface of the particle is described by a film resistance mechanism:

$$\frac{dq_i}{dt} = aK_f(C_i - C_i^*) \tag{A6}$$

where a $(=3/R_0)$ is the interfacial area per unit volume of the adsorbent particles, R_0 is the radius of the particle, K_f is the liquid field mass transfer coefficient and C_i^* is the intermediate concentration of the adsorbate in the liquid phase at the surface of the particles.

The interaction between the adsorbate and the immobilized ligand at the particle surface is described by the second-order reversible equation

$$\frac{dq_i}{dt} = k_1[(q_m - q_i)C_i^* - K_d q_i] \tag{A7}$$

where k_1 is the forward interaction rate constant, q_m is the maximum adsorption capacity of the immobilized ligand and K_d is the adsorption equilibrium constant. At equilibrium, Eq. A7 becomes the Langmuir isotherm equation.

Eliminating C_i^*, q_i and its derivative from Eqs. A3, A5, A6 and A7, the rate of change of C_i with time can be written as follows:

$$-\left(\frac{1}{M} + \frac{1}{k_1}\right)\frac{dC_i}{dt} = (C_i - x_1)(C_i - x_2) \tag{A8}$$

where

$$M = \frac{A}{R_v q_m - C_{T,i} + C_i} \tag{A9}$$

and

$$A = aK_f R_v \tag{A10}$$

x_1 and x_2 are the roots of the quadratic equation

$$C_i^2 - BC_i - K_d C_{T,i} = 0 \tag{A11}$$

where

$$B = C_{T,i} - R_v q_m - K_d \tag{A12}$$

and

$$x_1 = \frac{1}{2}[B + \sqrt{B^2 + 4K_d C_{T,i}}] \tag{A13}$$

$$x_2 = \frac{1}{2}[B - \sqrt{B^2 + 4K_d C_{T,i}}] \tag{A14}$$

Eq. A8 can be directly integrated to yield

$$\left(C_{T,i} - R_v q_m - \frac{A}{k_1}\right) \ln\left(\frac{C_i - x_1}{C_i - x_2}\frac{C_{i,0} - x_2}{C_{i,0} - x_1}\right) - x_1 \ln\left(\frac{C_i - x_1}{C_{i,0} - x_1}\right) + x_2 \ln\left(\frac{C_i - x_2}{C_{i,0} - x_2}\right) = A(x_1 - x_2)\,\Delta t \tag{A15}$$

Eq. A15 can be used to calculate the liquid-phase concentration at the end of each time increment Δt for section i. In this equation and also in Eq. A8 both the film mass transfer and surface interaction rates are considered finite.

Adsorption with porous adsorbent particles

Two additional assumptions were used for the porous particle case in the sectional model. One assumption is that a linear driving force approximation can be used to describe the mass transfer of the adsorbate in the liquid from the entrance of the pores at the external surface to the particle internal surface [15]. The second assumption is that the pore fluid can be assumed to be stagnant, and therefore only the bulk fluid was transferred to the next section at the end of each time increment.

The overall mass balance in section i is

$$\varepsilon C_i + (1-\varepsilon)\varepsilon_p C_{p,i} + (1-\varepsilon)(1-\varepsilon_p) q_i = [\varepsilon + (1-\varepsilon)\varepsilon_p] C_{T,i} \tag{A16}$$

where $C_{p,i}$ is the adsorbate concentration in the pore fluid and ε_p is the particle void fraction. Other symbols are the same as defined in Eq. A2. The unit of q_i is taken as the mass per unit volume of solid. With the linear driving force approximation the pore fluid can be treated as a mass transfer medium rather than a separate phase, thus enabling it to be combined with the bulk fluid in the overall mass balance [15]. Therefore, the pore fluid was lumped with the bulk fluid, i.e., $C_{p,i} = C_i$. Eq. A16 then becomes

$$[\varepsilon + (1-\varepsilon)\varepsilon_p] C_i + (1-\varepsilon)(1-\varepsilon_p) q_i = [\varepsilon + (1-\varepsilon)\varepsilon_p] C_{T,i} \tag{A17}$$

In this case, the value of $C_{T,i}$ can be calculated by Eq. A3, with the volume ratio of the solid phase to the liquid phase, R_v, becoming

$$R_v = \frac{1 - [\varepsilon + (1-\varepsilon)\varepsilon_p]}{\varepsilon + (1-\varepsilon)\varepsilon_p} \tag{A18}$$

and the value of $C_{i,0}$ is calculated as

$$C_{i,0} = \frac{\varepsilon}{\varepsilon + (1-\varepsilon)\varepsilon_p} \cdot C_{i-1} + \frac{(1-\varepsilon)\varepsilon_p}{\varepsilon + (1-\varepsilon)\varepsilon_p} \cdot C_i \tag{A19}$$

Eq. A19 indicates that at the end of each time increment, the pore fluid remained in the section, and only the bulk fluid in section $i-1$ was transferred to section i.

The differential form of Eq. A17 is then identical in form with Eq. A5. The solution for the case with porous particles can then be obtained with the same approach in Eqs. A5–A14. The differences are that an effective overall liquid-phase mass transfer coefficient, K_e, replaces K_f in Eqs. A6 and A10, and in Eqs. A6 and A7 C_i^* is redefined as the intermediate concentration of the adsorbate in the liquid phase at the internal surface of the particles. A more detailed discussion on these points has been presented previously [15].

Two simplified cases

As discussed in the case of a finite bath [15], two simplified cases for chromatographic packed beds may be considered. First, if the surface interaction rate constant k_1 is assumed to be infinite, the mass transfer becomes the rate-controlling step. As a result, when the forward rate constant for adsorption is very large Eq. A15 can be simplified to

$$(C_{T,i} - R_v q_m) \ln\left(\frac{C_i - x_1}{C_i - x_2}\frac{C_{i,0} - x_2}{C_{i,0} - x_1}\right) - x_1 \ln\left(\frac{C_i - x_1}{C_{i,0} - x_1}\right) + x_2 \ln\left(\frac{C_i - x_2}{C_{i,0} - x_2}\right) = A(x_1 - x_2)\,\Delta t \quad \text{(A20)}$$

This equation implies that equilibrium exists between the adsorbate and the adsorbate–ligand complex at each point on the particle surface and is referred to as the equilibrium case.

Second, if the mass transfer rate is very high, then the surface interaction (second-order kinetics) is considered as the rate-controlling step. As a result, Eq. A8 becomes

$$-\frac{1}{k_1}\cdot\frac{dC_1}{dt} = (C_i - x_1)(C_i - x_2) \quad \text{(A21)}$$

and the integrated form is

$$-\frac{1}{k_1}\ln\left(\frac{C_i - x_1}{C_i - x_2}\cdot\frac{C_{i,0} - x_2}{C_{i,0} - x_1}\right) = (x_1 - x_2)\,\Delta t \quad \text{(A22)}$$

This case can be referred to as the kinetic controlling case. In this case, the concentration of the adsorbate in the liquid phase as a function of time then can be expressed as

$$C_i = \frac{x_1(C_{i,0} - x_2) - x_2(C_{i,0} - x_1)\,e^{(x_2 - x_1)k_1\,\Delta t}}{(C_{i,0} - x_2) - (C_{i,0} - x_1)\,e^{(x_2 - x_1)k_1\,\Delta t}} \quad \text{(A23)}$$

which can be used directly to calculate the concentration in the liquid phase at time Δt. In the cases where the value of the liquid mass transfer coefficients are finite, i.e., Eqs. A15 or A20 is required, a bisectional method can be adopted to calculate the concentrations.

References

[1] M.T.W. Hearn, *Aust. J. Biotechnol.*, 3 (1989) 183.
[2] Y.D. Clonis, in J.A. Asenjo (Editor), *Separation Processes in Biotechnology*, Marcel Dekker, New York, 1990, p. 401.
[3] A. Jungbauer, *J. Chromatogr.*, 639 (1993) 3.
[4] J.-C. Janson and P. Hedman, *Biotechnol. Prog.*, 3 (1987) 9.
[5] G.H. Cowan, I.S. Gosling and W.P. Sweetenham, *J. Chromatogr.*, 484 (1989) 187.
[6] P. Dantigny, Y. Wang, J. Hubble and J.A. Howell, *J. Chromatogr.*, 545 (1991) 27.
[7] P.R. Levison, S.E. Badger, D.W. Toome, M.L. Koscielny, L. Lane and E.T. Butts, *J. Chromatogr.*, 590 (1992) 49.
[8] Q.M. Mao, I.G. Prince and M.T.W. Hearn, in I.G. Prince (Editor), *Proceedings of the 10th Australian Biotechnology Conference, Melbourne 4–7 February, 1992*, Australian Biotechnology Association, Melbourne, 1992, pp. 308–311.
[9] Q.M. Mao, I.G. Prince and M.T.W. Hearn, *J. Chromatogr.*, 646 (1993) 81.
[10] F.B. Anspach, A. Johnston, H.-J. Wirth, K.K. Unger and M.T.W. Hearn, *J. Chromatogr.*, 499 (1990) 103.
[11] H.-J. Wirth, K.K. Unger and M.T.W. Hearn, *Anal. Biochem.* 208 (1993) 16.
[12] H.-J. Wirth, *Ph.D. Dissertation*, Joh.-Gutenberg University, Mainz, 1990.
[13] A. Johnston, Q.M. Mao and M.T.W. Hearn, *J. Chromatogr.*, 548 (1991) 127.
[14] Q.M. Mao, A. Johnston, I.G. Prince and M.T.W. Hearn, *J. Chromatogr.*, 548 (1991) 147.
[15] Q.M. Mao, R. Stockmann, I.G. Prince and M.T.W. Hearn, *J. Chromatogr.*, 646 (1993) 67.
[16] D.D. Do, *AIChE J.*, 31 (1985) 1329.
[17] J. Hubble, *Biotechnol. Tech.* 3., (1989) 113.
[18] S. Yamamoto and Y. Sano, *J. Chromatogr.*, 597 (1992) 173.
[19] A.I. Liapis, B. Anspach, M.E. Findley, J. Davies, M.T.W. Hearn and K.K. Unger, *Biotechnol. Bioeng.*, 34 (1989) 467.
[20] B.J. Horstmann and H.A. Chase, *Chem. Eng. Res. Des.*, 67 (1989) 243.
[21] J. Xie, M.I. Aguilar and M.T.W. Hearn, *J. Chromatogr. A*, 691 (1995) 263.